IEICE TRANSACTIONS

on Communications

VOL. E98-B NO. 8
AUGUST 2015

A PUBLICATION OF THE COMMUNICATIONS SOCIETY

The Institute of Electronics, Information and Communication Engineers
Kikai-Shinko-Kaikan Bldg., 5-8, Shibakoen 3chome, Minato-ku, TOKYO, 105-0011 JAPAN

IEICE TRANS. COMMUN., VOL.E98–B, NO.8 AUGUST 2015

PAPER

Adaptive Multi-Rate Designs and Analysis for Hybrid FSO/RF Systems over Fading Channels*

Vuong V. MAI[†a)], ***Student Member and*** **Anh T. PHAM**[†], ***Member***

SUMMARY This paper proposes the concept of adaptive multi-rate (AMR), which jointly employs switching between two links and adaptive rate on each link, for hybrid free-space optical/radio-frequency (FSO/RF) systems. Moreover, we present the cross-layer design of AMR switching, which is based on both the physical and link layers with an automatic-repeat request (ARQ) scheme. We develop an analytical framework based on a Markov chain model for system performance analysis. System performance metrics, including frame-error rate, goodput and link switching probability, are analytically studied over fading channels. Numerical results quantitatively show how the proposal significantly outperforms conventional ones with physical layer-based design and/or fixed-rate switching operation.

key words: *hybrid FSO/RF, turbulence channel, automatic-repeat request (ARQ), adaptive multi-rate (AMR)*

1. Introduction

Free-space optical (FSO) communication is a wireless optical communication technology based on the propagation of light in free space. Achieving data rates comparable to fiber optics without incurring exorbitant costs and requiring significant amount of time for installation, FSO communication systems are able to provide low-cost, time-constrained and high-bandwidth connectivity in various network scenarios. However, several issues have hampered the practical deployment of FSO systems. Caused by variations of the air refractive-index due to solar heating and wind, atmospheric turbulence results in rapid fluctuations in both intensity and phase of received signals [1]. In addition, FSO systems experience significant deterioration in the presence of fog; even a moderate fog can cause 40 dB/km attenuation [2]. These issues degrade the reliability and availability of systems.

Recently, the integration of FSO and RF links has been introduced in communication networks for achieving high reliability and availability. This is logical due to the fact that these systems are not affected in the same way by transmission media. In FSO links, the main degrading factors are fog and atmospheric turbulence, whereas rain does not influence notably. On the contrary, RF links are susceptible to heavy rain conditions, but not fog or atmospheric effects [2]–[4].

There are basically two main types of hybrid RF/FSO implementations: (i) simultaneous transmission systems, and (ii) switchover systems. In the simultaneous transmission systems, data is duplicated and transmitted simultaneously over both links [3], [5]–[7]. Though the simultaneous transmission systems offer high reliability, RF link resources are, in principle, wasted whenever the FSO link is in normal operation. Our study therefore focuses on the switchover systems, and we presume that the FSO link is favourable due to the fact that it potentially has higher data rate, better energy efficiency, and the possibility to be compatible with fiber-optic systems. In the considered system, the RF link works as a standby backup connection, and traffic is switched to this link only when the primary FSO link is down [2], [8]–[11].

Previously proposed switchover systems were based on two fixed transmission modes. Consequently, these systems become sensitive to short-term changes in the environment, such as atmospheric turbulences. Reported in [9], even in clear days switching between the FSO and RF links may happen very frequently, which can lead to the degradation of system throughput and availability. Therefore, to improve the system performance under the impact of environmental short-term changes, it is preferable that the hybrid systems are employed more adaptive characteristics.

Motivated by link adaptation schemes, which have been employed in RF wireless systems [12], [13], and recently introduced for FSO systems [14]–[16], we propose adaptive multi-rate (AMR) scheme for hybrid FSO/RF switchover systems, which jointly employs switching between two links and adaptive rate on each link. In particular, unlike conventional systems, which directly switch from a high data transmission rate of FSO link to a lower rate of RF link when FSO channel quality degrades [2], [8]–[11], the proposed system gradually reduces data rate in FSO link, and only switches to RF link in the worst scenario. When the system works on the RF link, transmission rate is also chosen according to the RF channel states.

Furthermore, one of the most critical issues when applying AMR in switchover systems is to design switching thresholds, which are used for either link switching or adaptive rate decisions. Conventionally, within the context of FSO communications, the switching design is based on the performance of physical layer for either link switching [2], [8]–[11] or adaptive rate decisions [14]–[16]. In this study, we employ the cross-layer design approach for AMR switching that bases on the joint performance of physical and link layers with automatic-repeat request (ARQ), an ef-

Manuscript received November 24, 2014.
Manuscript revised March 29, 2015.

[†]The authors are with the Computer Communications Lab., The University of Aizu, Aizuwakamatsu-shi, 965-8580 Japan.

*The paper has been presented in part at IEEE GLOBECOM OWC 2014.

a) E-mail: m.v.vuong@ieee.org

DOI: 10.1587/transcom.E98.B.1660

ficient control mechanism for reliable transmissions in the link layer [17]–[19].

To study the system performance, we newly develop an analytical framework based on Markov chain model, which reflects both link switching and adaptive rate operations. We then analytically study the performance of proposed systems, in terms of frame-error rate, goodput and link switching probability, over fading channels. Numerical results confirm the superiority of AMR schemes over conventional designs, and that the cross-layer design is more efficient than physical layer-based one.

The remainder of the paper is organized as follows. The system descriptions are described in Sect. 2. In Sect. 3, the concepts of AMR and threshold designs are presented. The AMR Markov chain model and performance metrics are presented in Sects. 4 and 5, respectively. The numerical results are given in Sect. 6. Finally, Sect. 7 concludes the paper.

Notation: $\Gamma(.)$, $\Gamma_l(.,.)$ and $\Gamma_u(.,.)$ are the ordinary Gamma, the lower incomplete Gamma and the upper incomplete Gamma functions, respectively; $K_v(.)$ is the modified Bessel function of second kind and order v-th; $I_0(.)$ is the zero order modified Bessel function of the first kind; $Q_M(.,.)$ is the Marcum function; $B(.,.)$ is the Beta function; erfc(.) and erfcinv(.) are the complementary error function and its inverse function.

2. System Descriptions

Figure 1 shows a point-to-point hybrid FSO/RF system including two individual line-of-sight (LOS) FSO and RF channels. The changes in the environment that affect on the quality of channels can be divided into two kinds: (i) long-term change caused by fog and/or rain: which is in order of hours and depends on seasons, and (ii) short-term change caused by fading: which is in order of milliseconds, may happen daily. Originally, switching between FSO and RF link is proposed to again the effects of long-term changes. However, in current systems, the link switching may happen frequently due to the effect of short-term one. In this study, we therefore mainly focus on short-term change caused by the fading channels.

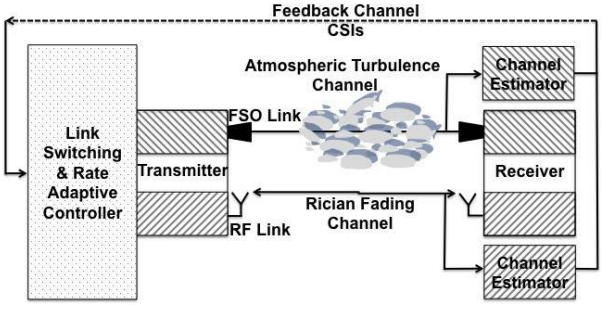

Fig. 1 Hybrid FSO/RF system model with adaptive multi-rate scheme.

2.1 Channel Models

2.1.1 FSO Channel

The Gamma-Gamma distribution is generally accepted for describing the turbulence-induced fading, h_f, whose probability density function (pdf) is given by

$$f_{H_f}(h_f) = \frac{2(\alpha\beta)^{\frac{\alpha+\beta}{2}}}{\Gamma(\alpha)\Gamma(\beta)} h_f^{\frac{\alpha+\beta}{2}-1} K_{\alpha-\beta}\left(2\sqrt{\alpha\beta h_f}\right), \quad (1)$$

where the pdf parameters α and β are given by

$$\alpha = \left\{\exp\left[\frac{0.49\sigma_R^2}{\left(1+1.11\sigma_R^{12/5}\right)^{7/6}}\right]-1\right\}^{-1},$$
$$\beta = \left\{\exp\left[\frac{0.51\sigma_R^2}{\left(1+0.69\sigma_R^{12/5}\right)^{5/6}}\right]-1\right\}^{-1}. \quad (2)$$

Here, σ_R^2 is the Rytov variance, which is dependent upon the link distance and the refractive index structure parameter. Typically, weak turbulence fluctuations are associated with $\sigma_R^2 < 1$, moderate with $\sigma_R^2 \approx 1$, strong with $\sigma_R^2 > 1$, and the saturation regime is defined by $\sigma_R^2 \to \infty$ [14].

2.1.2 RF Channel

As a requirement for the FSO communications, a LOS path always exists. Hence, the fading gain h_r of RF channel is assumed to be modeled by a Rician distribution,

$$f_{H_r}(h_r) = \frac{h_r}{\sigma_r^2}\exp\left(-\frac{h_r^2+s^2}{2\sigma_r^2}\right) I_0\left(\frac{h_r s}{\sigma_r^2}\right), \quad (3)$$

where $2\sigma_r^2$ is the mean power of the sum of the non-specular component, and s^2 is the LOS component. We can rewrite (3) as

$$f_{H_r}(h_r) = 2(K+1)h_r \exp\left(-K-(K+1)h_r^2\right) \times I_0\left(2h_r\sqrt{K(K+1)}\right), \quad (4)$$

where $K = s^2/2\sigma_r^2$, is the Ricean factor that depends on various link parameters, such as link distance and antenna height [20].

2.2 SNR Statistics

We define the instantaneous received signal-to-noise ratio (SNR) of FSO and RF links as

$$\gamma_f = \overline{\gamma}_f h_f^2, \text{ and } \gamma_r = \overline{\gamma}_r h_r^2, \quad (5)$$

where $\overline{\gamma}_f$ and $\overline{\gamma}_r$ are the average electrical SNR per symbol of FSO and RF links, respectively.

For FSO link: : Using (1) and (5), after transformation of random variable h_f, we obtain the pdf of γ_f as

$$f_{\gamma_f}(\gamma_f) = \frac{(\alpha\beta)^{\frac{\alpha+\beta}{2}}}{\Gamma(\alpha)\Gamma(\beta)\overline{\gamma}_f^{\frac{\alpha+\beta}{4}}}\gamma_f^{\frac{\alpha+\beta}{4}-1}K_{\alpha-\beta}\left(2\sqrt{\alpha\beta\sqrt{\frac{\gamma_f}{\overline{\gamma}_f}}}\right), \tag{6}$$

while its cumulative distribution function (cdf) can be expressed as [6]

$$F_{\gamma_f}(\gamma_f) = \frac{1}{\Gamma(\alpha)\Gamma(\beta)}G_{1,3}^{2,1}\left[\alpha\beta\sqrt{\frac{\gamma_f}{\overline{\gamma}_f}}\Bigg|_{\alpha,\beta,0}^{1}\right]. \tag{7}$$

For RF link: According to [20], the pdf and cdf of γ_r are given by

$$f_{\gamma_r}(\gamma_r) = \frac{K+1}{\overline{\gamma}_r}\exp\left(-K-(K+1)\frac{\gamma_r}{\overline{\gamma}_r}\right) \times I_0\left(2\sqrt{K(K+1)\frac{\gamma_r}{\overline{\gamma}_r}}\right), \tag{8}$$

$$F_{\gamma_r}(\gamma_r) = 1 - Q_M\left(\sqrt{2K}, \sqrt{\frac{2(K+1)\gamma_r}{\overline{\gamma}_r}}\right). \tag{9}$$

3. Adaptive Multi-Rate

3.1 Adaptive Multi-Rate Concept

As Eq. (5) captures the nature of fading channels, the channel condition can be reflected by the instantaneous received SNR. In Fig. 1, the channel state information (CSIs) refer to the values of γ_f and γ_r. They can be estimated at the receiver and fed back to the transmitter via a dedicated feedback link. In hybrid RF/FSO systems, to improve the utility of RF link, it can be used as the feedback link to enable CSI knowledge at the transmitter[†]. The scintillation fading process, the coherence time of scintillation in order of 10^{-2} to 10^{-3} seconds, is slow compared to the data rates typical of optical transmission. The coherence time of fading experienced by RF channel is also in order of 10^{-1} to 10^{-2} seconds (for the LOS path and the fixed transmitter/receiver). Due to these slowly time-varying nature of fading channels, CSIs are still up-to-date information when arriving the transmitter [3].

Based on the information, the switching between two links and adaptive rate in each link can be adjusted dynamically at the transmitter. This is the main concept of proposed AMR scheme.

3.1.1 Link Switching Operation

Transmissions occur cycle-by-cycle. Due to the fact that FSO link works as the primary link in the system, the cycle length is set to be equal the coherence time of scintillation. At the begging of a cycle, the system first has to decide the transmission link. The FSO link will be used as long as its link quality is above a certain threshold. Otherwise, the system will resort to the RF link. To support link switching decision, the CSI of FSO link is considered, a SNR threshold, γ_{th}, is chosen as the link switching threshold. The threshold is selected based on the lowest transmission rate of FSO link, which is discussed later in Sect. 3.1.3. At cycle n, we denote the link selected for transmitting data as X_n.

$$X_n = \begin{cases} \text{FSO}, & \gamma_{th} \le \gamma_f < \infty, \\ \text{RF}, & 0 \le \gamma_f < \gamma_{th}. \end{cases} \tag{10}$$

3.1.2 Adaptive Rate Operation

After deciding the transmission link, the system chooses the transmission rate depending on selected link's CSI. We assume that, for FSO and RF links, there are respectively $\mathfrak{n}$ and $\mathfrak{m}$ available transmission rate levels, which are arranged as

$$\begin{aligned} \mathfrak{R}^f &= \left\{\mathfrak{R}_{f1}, \mathfrak{R}_{f2}, ..., \mathfrak{R}_{f\mathfrak{n}}\right\}, \\ \mathfrak{R}^r &= \left\{\mathfrak{R}_{r1}, \mathfrak{R}_{r2}, ..., \mathfrak{R}_{r\mathfrak{m}}\right\}. \end{aligned} \tag{11}$$

We also divide, respectively, the range of FSO SNR and RF SNR into $(\mathfrak{n}+1)$ and $(\mathfrak{m}+1)$ set of non-overlapping intervals defined by the partition.

$$\begin{aligned} \Gamma^f &= \left\{[\gamma_{f0}, \gamma_{f1}), [\gamma_{f1}, \gamma_{f2}), ..., [\gamma_{f\mathfrak{n}}, \gamma_{f(\mathfrak{n}+1)})\right\}, \\ \Gamma^r &= \left\{[\gamma_{r0}, \gamma_{r1}), [\gamma_{r1}, \gamma_{r2}), ..., [\gamma_{r\mathfrak{m}}, \gamma_{r(\mathfrak{m}+1)})\right\}, \end{aligned} \tag{12}$$

where $\gamma_{f0} = \gamma_{r0} = 0$ and $\gamma_{f(\mathfrak{n}+1)} = \gamma_{r(\mathfrak{m}+1)} = \infty$. Each interval is associated with a transmission rate according to the following rule.

When the FSO link is selected:

$$R = \mathfrak{R}_{fj},\ \gamma_{fj} \le \gamma_f < \gamma_{f(j+1)}. \tag{13}$$

When the RF link is selected:

$$R = \begin{cases} \mathfrak{R}_{ri}, & \gamma_{ri} \le \gamma_r < \gamma_{r(i+1)}, \\ 0, & \gamma_{r0} \le \gamma_r < \gamma_{r1}. \end{cases} \tag{14}$$

Note that $R = 0$ refers to the case where no data are transmitted.

3.1.3 AMR

To combine the operation of link switching and adaptive rate, γ_{th} is set to γ_{f1}, the threshold corresponding to lowest transmission rate in the FSO link. Now the system can run AMR based on a look-up table as illustrated in Fig. 2 (an example when $\mathfrak{m} = \mathfrak{n} = 5$). In addition, to control the transmission rate, we employ adaptive modulation in our system. As FSO systems typically use pulse-based modulations, while phase modulations are preferred in RF systems, we assume that N-PAM ($N = 2^j, j = 1, 2, ..., \mathfrak{n}$) with a symbol rate of R_f is used in FSO link, while M-QAM

[†]Another option is having an independent feedback channel for each link due to the fact that both commercially available FSO and RF units have full-duplex capabilities and a small portion of the large available bandwidth can be allocated for feedback purposes without much effect on data rates.

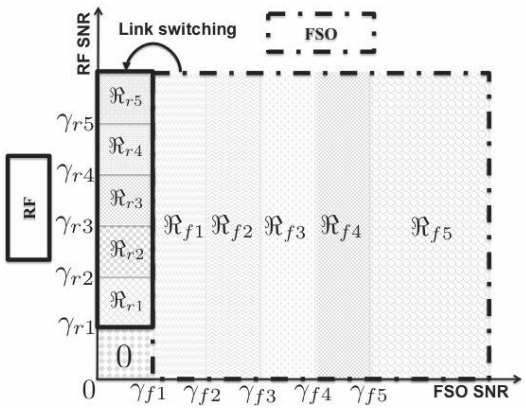

Fig. 2 Example of look-up table when $\mathfrak{m} = \mathfrak{n} = 5$.

$(M = 2^i, i = 1, 2, ..., \mathfrak{m})$ with a symbol rate of R_r is adopted in RF link[†]. The transmission rate is then given as

$$\Re_{fj} = jR_f \text{ and } \Re_{ri} = iR_r. \tag{15}$$

Here, for the fixed symbol rate, in order to change the transmission rate, we can change the signal constellation size. Practically, this flexibility could be addressed via a software-based configuration or implementation of the operating function at the transmitter [21].

3.2 Switching Thresholds Designs

This section discusses one of the most critical issues when applying AMR in the system: how to design switching thresholds (i.e., γ_{fj} and γ_{ri}). Firstly, we introduce the conventional design, which is based on the performance of physical layer. Secondly, to further improve the system performance, we employ the cross-layer design approach that bases on the joint performance of physical layer and link layer with ARQ.

3.2.1 Physical Layer-Based Design

The aim of AMR is to provide the highest possible transmission rate while maintaining a required quality of service (QoS). In physical layer based design, a target bit-error rate (BER_0) is considered as the common level of required QoS for both links. So, the problem can be formally formulated as

$$\begin{aligned} &\max\ R \mid R \in \left\{0, R_r, ..., \mathfrak{m}R_r, R_f, ..., \mathfrak{n}R_f\right\} \\ &\text{subject to } \text{BER}_R \le \text{BER}_0 \end{aligned} \tag{16}$$

where BER_R is the conditional BER of system whose transmission rate is R. BER_R is calculated based on the conditional BER of N-PAM or M-QAM over the Additive white Gaussian noise (AWGN) channel, which is well approximated by [14] and [12], as follows

$$\text{BER}(N, \gamma_f) \cong \frac{N-1}{N\log_2 N}\text{erfc}\left(\sqrt{\frac{3\gamma_f}{2(N-1)(2N-1)}}\right), \tag{17}$$

$$\text{BER}(M, \gamma_r) \cong 0.2\exp\left[-\frac{3\gamma_r}{2(M-1)}\right]. \tag{18}$$

From (16)–(18), the switching thresholds are derived as

$$\gamma_{fj} = \frac{2(2^j-1)(2^{j+1}-1)}{3}\left[\text{erfcinv}\left(\frac{2^j j\text{BER}_0}{2^j-1}\right)\right]^2, \tag{19}$$

$$\gamma_{ri} = \frac{-2(2^i-1)}{3}\ln(5\text{BER}_0). \tag{20}$$

3.2.2 AMR/ARQ Cross-Layer Design

This design takes into account the error control ability of ARQ, and uses a target link layer frame-error rate (FER_0) as the required QoS. This is expected to improve overall system performance as in fact when ARQ is employed, the system is stronger, and it may stay longer in the FSO link under the presence of atmospheric turbulence.

We first consider the conditional frame-error rate (FER_R), where frames are formed with l transmitted bits. Without any coding on this frame, the probability of a frame error at a given instantaneous SNR is given as

$$\text{FER}_R(\gamma) = 1 - [1 - \text{BER}_R(\gamma)]^l, \ \ \gamma \in \left\{\gamma_f, \gamma_r\right\}. \tag{21}$$

By applying a probability union-bound, we have: $1 - [1 - \text{BER}_R(\gamma)]^l \le l\text{BER}_R(\gamma)$. The bound gets tighter as $\text{BER}_R(\gamma)$ decreases when $\gamma \to \infty$. So, we can derive an approximation for the conditional FER as follows

$$\text{FER}(N, \gamma_f) \cong l\text{BER}(N, \gamma_f), \tag{22}$$

$$\text{FER}(M, \gamma_r) \cong l\text{BER}(M, \gamma_r). \tag{23}$$

Notice that the probability union-bound can be also used to find the connection between the target link layer FER and the target BER, this is: $\text{FER}_0 = 1 - (1 - \text{BER}_0)^l \approx l\text{BER}_0$.

Next, we determine how to design the switching thresholds, considering that ARQ is implemented in the link layer. We set the maximum number of ARQ re-transmissions (i.e., the persistence level) to Ł. It means that a frame is considered to be lost only if it does not get through the links after (Ł + 1) transmissions. To this end, the conventional FER_0 can be translated into a new equivalent link layer target FER of $\text{FER}_0^{1/(Ł+1)}$. So, the switching thresholds can be designed based on the following conditions

$$\begin{aligned} &\max\ R \mid R \in \left\{0, R_r, ..., \mathfrak{m}R_r, R_f, ..., \mathfrak{n}R_f\right\} \\ &\text{subject to } \text{FER}_R \le \text{FER}_0^{\frac{1}{Ł+1}}. \end{aligned} \tag{24}$$

Finally, from (22)–(24), the switching thresholds are derived as

$$\gamma_{fj} = \frac{2(2^j-1)(2^{j+1}-1)}{3}\left[\text{erfcinv}\left(\frac{2^j j\text{FER}_0^{\frac{1}{Ł+1}}}{l(2^j-1)}\right)\right]^2, \tag{25}$$

[†]These two modulation formats are selected as an illustrative example. However, the proposed scheme is applicable to arbitrary multilevel modulations.

$$\gamma_{ri} = \frac{-2(2^i - 1)}{3} \ln\left(\frac{5\mathrm{FER}_0^{\frac{1}{\text{Ł}+1}}}{l}\right). \quad (26)$$

Note that (19) and (20) are the special cases of (25) and (26) when Ł = 0.

Figure 3 compares the FER exact expression obtained by (21) with its approximations obtained by (22), and justifies the use of the FER approximations. Figure 3(a) also illustrates an example of how to obtain the switching thresholds for variable values of Ł. Specifically, from the crossover points found on the curves of $\mathrm{FER}_0^{1/(\text{Ł}+1)}$ with the curves of $\mathrm{FER}(N, \gamma_f)$, we can find the corresponding values of the thresholds. Obviously, when increasing the value of Ł, the set of thresholds tends to be shifted to the left. As a result, (i) the region that the system works on FSO link (i.e., $[\gamma_{f1}, \infty)$) is extended, and (ii) the region that the system works with high data rate (i.e., $[\gamma_{f5}, \infty)$) is extended.

In summary, for a given practical system, the following parameters are known: the number of available transmission rates ($\mathfrak{n}$, $\mathfrak{m}$), the symbol rates (R_f, R_r), the levels of required QoS (BER_0, FER_0), the frame length (l), the persistence level (Ł). The concept of AMR and its designs can be applied to the system as follows

- Creating the look-up table: the sets of transmission rates ($\mathfrak{R}^f$, $\mathfrak{R}^r$) in (11) are *pre-designed* based on (15); the sets of thresholds (Γ^f, Γ^r) in (12) are *pre-designed* based on (19), (20) for the physical layer-based design or (25), (26) for the AMR/ARQ cross-layer design. Figure 2 is an example of look-up table.
- Running AMR: At the beginning of a cycle, the receiver fed back to the transmitter CSIs (γ_f, γ_r), system runs AMR by following two steps: (i) deciding the transmission link based on (10), and (ii) deciding the transmission rate based on (13) if FSO link is selected or (14) if RF link is selected.

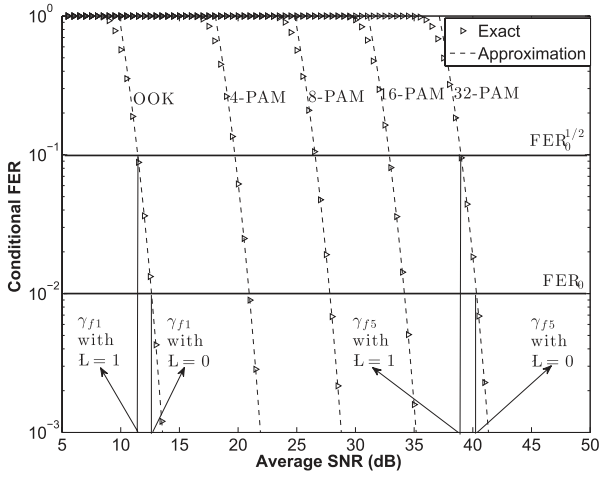

(a) N-PAM ($N = 2^j, j = 1, 2, 3, 4, 5$) in FSO link.

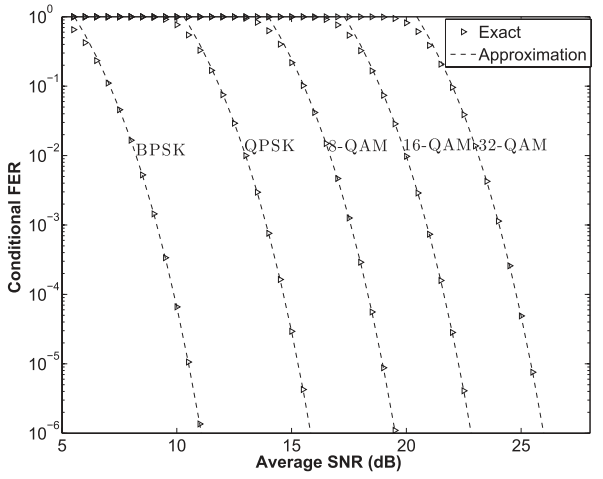

(b) M-QAM ($M = 2^i, i = 1, 2, 3, 4, 5$) in RF link.

Fig. 3 Exact and approximate FERs for the AWGN channel when l = 1080 bits.

4. Markov Chain Models

In this section, to analytically study the system performance, we newly develop a Markov chain model, which reflects both link switching and adaptive rate operations. Furthermore, in the model, we investigate the time-varying behavior of atmospheric turbulence, which was often omitted in modeling either link switching [8] or adaptive rate [14]–[16]. However, as in AMR operation, we observe frame-by-frame transmissions that capture the memory properties of channel, it is important to include the time-varying behavior of atmospheric turbulence for more accurate performance evaluation. Experimental results supporting the time-varying behavior model can be found in [22] for the atmospheric turbulence.

4.1 Markov Chain Model for AMR

The operation of AMR can be modeled as the Markov chain, as shown in Fig. 4. There are two phases (i.e., FSO and RF) and ($\mathbb{N} = \mathfrak{n}+\mathfrak{m}+1$) states arranged in order, $1 \to \mathbb{N}$, from left to right. Each state expressing different transmission rates, and the transmission rate decreases gradually from left to right. Under a slow fading channel, we can assume that the transitions only happen between adjacent states.

Initially, the system works in FSO phase with the highest-rate mode (leftmost mode). Whenever the FSO channel quality degrades, the system moves to a lower-rate mode. In cases when the channel quality does not change

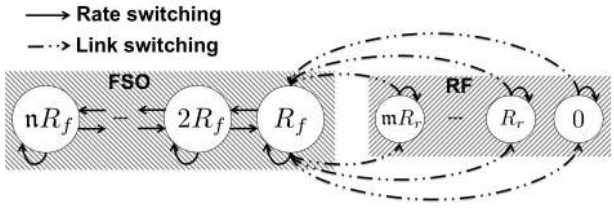

Fig. 4 The Markov chain for AMR operation.

(or gets better), the system stays at the current mode (or goes back the previous higher-rate mode). At the lowest-rate mode of FSO phase, the system switches to RF phase if the FSO channel quality continues to degrade. At this time, based on the current channel quality of RF link, the system selects the one having the most suitable rate from $\mathfrak{m}$ available modes. When the system stays in RF link, as the coherence time of RF channel is much longer than that of FSO channel (refer to Sect. 3.1), we further assume that the RF channel state is constant with regard to that of FSO, i.e. there is no state transition between two states in the RF phase. Finally, right after the FSO channel is available, the system goes back to FSO phase and increases rate gradually from the lowest-rate mode

Obviously, in the Markov chain, there are four kinds of state transition: (i) inside FSO phase, (ii) inside RF phase, (iii) from FSO phase to RF phase, and (iv) from RF phase to FSO phase. So, we construct a $\mathbb{N}\times\mathbb{N}$ state transition matrix as follows

$$\mathbf{Q}=\left[\begin{array}{c|c}\mathbf{Q}_{FSO\to FSO} & \mathbf{Q}_{FSO\to RF}\\ \hline \mathbf{Q}_{RF\to FSO} & \mathbf{Q}_{RF\to RF}\end{array}\right]. \tag{27}$$

4.1.1 Basic State Transition Analysis

To calculate the elements of the matrix, we first consider a basic diagram for analyzing the state transition in Fig. 5. Let $\gamma_{k-1}<\gamma_k<\gamma_{k+1}<\gamma_{k+2}$ be the thresholds of SNR. The system is said to be in the state $S(k)$ if the received SNR is in the interval $[\gamma_k,\gamma_{k+1})$. To characterize the time-varying behavior, at any threshold level of γ_{th}, there is a function of level crossing rate (LCR), $N(\gamma_{th})$, which is defined as the average number of times per second that the received SNR of system passes (either upward or downward) the level of γ_{th}. In addition, let $T=l/R$ be the frame transmission time, where R is the transmission rate and l is the frame size. Now, the transition probabilities between $S(k)$ and its neighboring states are given as

$$\begin{aligned}p_{k,k+1}&=\frac{N(\gamma_{k+1})T}{\Pr(\gamma_k)},\ p_{k,k-1}=\frac{N(\gamma_k)T}{\Pr(\gamma_k)},\\ p_{k,k}&=1-p_{k,k+1}-p_{k,k-1},\end{aligned} \tag{28}$$

where $\Pr(\gamma_k)$ is the probability that the state $S(k)$ is selected, and thus computed as

$$\Pr(\gamma_k)=\int_{\gamma_k}^{\gamma_{k+1}} f_\gamma(\gamma)d\gamma=F_\gamma(\gamma_{k+1})-F_\gamma(\gamma_k), \tag{29}$$

where f_γ and F_γ are the pdf and cdf of γ [23]. To apply (28) into further analysis, we need to know LCR. Based on the experimental results supporting the time-varying behavior models, the LCR is inversely proportional to the coherence time, t_0, yet increases as the turbulence becomes stronger, and can obtained as follows [22]

$$N(\gamma_f)=\frac{1}{4\pi t_0}\exp\left(\frac{1}{2\left(1-e^{4\sigma_S^2}\right)}\left(\frac{\gamma_f-\overline{\gamma}_f}{\overline{\gamma}_f}\right)^2\right), \tag{30}$$

where σ_S^2 is log intensity variance, which describes the strength of turbulence. The relation between σ_S^2 and σ_R^2 is given by Eq. (10) of [24].

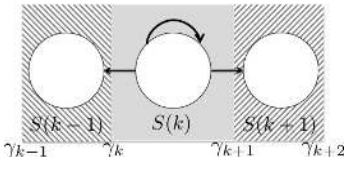

Fig. 5 A basic diagram for analyzing the state transition.

4.1.2 Sub-Matrix $Q_{FSO\to FSO}$

Considering the transition between states inside FSO phase, the following $\mathfrak{n}\times\mathfrak{n}$ state transition matrix can be used

$$\begin{aligned}&\mathbf{Q}_{FSO\to FSO}\\ &=\begin{bmatrix}\mathbf{ff}_{\mathfrak{n},\mathfrak{n}} & \mathbf{ff}_{\mathfrak{n},\mathfrak{n}-1} & 0 & 0 & \cdots & 0 & 0\\ \mathbf{ff}_{\mathfrak{n}-1,\mathfrak{n}} & \mathbf{ff}_{\mathfrak{n}-1,\mathfrak{n}-1} & \mathbf{ff}_{\mathfrak{n}-1,\mathfrak{n}-2} & 0 & \cdots & 0 & 0\\ 0 & \mathbf{ff}_{\mathfrak{n}-2,\mathfrak{n}-1} & \mathbf{ff}_{\mathfrak{n}-2,\mathfrak{n}-2} & \mathbf{ff}_{\mathfrak{n}-2,\mathfrak{n}-3} & \cdots & 0 & 0\\ 0 & 0 & \mathbf{ff}_{\mathfrak{n}-3,\mathfrak{n}-2} & \mathbf{ff}_{\mathfrak{n}-3,\mathfrak{n}-3} & \cdots & 0 & 0\\ \vdots & \vdots & \vdots & \vdots & \ddots & \vdots & \vdots\\ 0 & 0 & 0 & 0 & \cdots & \mathbf{ff}_{2,2} & \mathbf{ff}_{2,1}\\ 0 & 0 & 0 & 0 & \cdots & \mathbf{ff}_{1,2} & \mathbf{ff}_{1,1}\end{bmatrix},\end{aligned} \tag{31}$$

where $\mathbf{f}_{j,k}$ $(1\le j,k\le\mathfrak{n})$ is the probability that our system moves from a transmission rate of (jR_f) to one of (kR_f) and it is given as

$$\begin{aligned}&\mathbf{ff}_{j,k}\\ &=\begin{cases}0, & |k-j|\ge 2\\ \frac{N(\gamma_{f(j+1)})T_f^{(j)}}{\Pr(\gamma_{fj})}, & k=j+1\\ \frac{N(\gamma_{fj})T_f^{(j)}}{\Pr(\gamma_{fj})}, & 1\le j=k+1\le\mathfrak{n}\\ 1-\mathbf{ff}_{j,j+1}-\mathbf{ff}_{j,j-1}, & k=j\ne\mathfrak{n}\\ 1-\mathbf{ff}_{\mathfrak{n},\mathfrak{n}-1}, & k=j=\mathfrak{n}\end{cases},\end{aligned} \tag{32}$$

where $T_f^{(j)}=l/(jR_f)$ is the frame transmission time with the rate of jR_f.

4.1.3 Sub-Matrix $Q_{FSO\to RF}$

For transitions from FSO phase to RF phase, we consider a $\mathfrak{n}\times(\mathfrak{m}+1)$ state transition matrix and its elements as follows

$$\mathbf{Q}_{FSO\to RF}=\begin{bmatrix}0 & 0 & \cdots & 0\\ \vdots & \vdots & \ddots & \vdots\\ 0 & 0 & \cdots & 0\\ \mathbf{fr}_{1,\mathfrak{m}} & \mathbf{fr}_{1,\mathfrak{m}-1} & \cdots & \mathbf{fr}_{1,0}\end{bmatrix}. \tag{33}$$

Obviously, the transitions only come from the lowest-rate state of FSO phase. There are two simultaneous conditions for this transition: (i) γ_f of FSO link moves from $[\gamma_{f1},\gamma_{f2})$ to $[0,\gamma_{f1})$, and (ii) RF link has γ_r in $[\gamma_{ri},\gamma_{r(i+1)})$. Consequently, we obtain

$$\mathbf{fr}_{1,i} = \frac{N(\gamma_{f1})T_f^{(1)}}{\Pr(\gamma_{f1})}\Pr(\gamma_{ri}),\ \forall\, 0 \le i \le \mathrm{m}. \tag{34}$$

4.1.4 Sub-Matrix $Q_{RF\to FSO}$

The transitions from RF phase to FSO phase only depend on FSO link quality. The condition is that γ_f of FSO link moves from $[0, \gamma_{f1})$ to $[\gamma_{f1}, \gamma_{f2})$.

$$\mathbf{Q}_{RF\to FSO} = \begin{bmatrix} 0 & \cdots & 0 & \mathbf{rf}_{0,1} \\ 0 & \cdots & 0 & \mathbf{rf}_{1,1} \\ \vdots & \ddots & \vdots & \vdots \\ 0 & \cdots & 0 & \mathbf{rf}_{\mathrm{m},1} \end{bmatrix}, \tag{35}$$

where

$$\mathbf{rf}_{i,1} = \frac{N(\gamma_{f1})T_r^{(i)}}{\Pr(\gamma_{f0})},\ \forall\, 0 \le i \le \mathrm{m}, \tag{36}$$

where $T_r^{(i)} = l/(iR_r)$ is the frame transmission time with the rate of iR_r.

4.1.5 Sub-Matrix $Q_{RF\to RF}$

As mentioned, there is no state transition between two states in RF phase. Only self-transition happens in a state of RF phase when the system does not go back FSO phase. This is expressed by the condition of $(1 - \mathbf{rf}_{i,1})$.

$$\mathbf{Q}_{RF\to RF} = \begin{bmatrix} \mathbf{rr}_{\mathrm{m},\mathrm{m}} & 0 & 0 & 0 & \cdots & 0 & 0 \\ 0 & \mathbf{rr}_{\mathrm{m}-1,\mathrm{m}-1} & 0 & 0 & \cdots & 0 & 0 \\ 0 & 0 & \mathbf{rr}_{\mathrm{m}-2,\mathrm{m}-2} & 0 & \cdots & 0 & 0 \\ 0 & 0 & 0 & \mathbf{rr}_{\mathrm{m}-3,\mathrm{m}-3} & \cdots & 0 & 0 \\ \vdots & \vdots & \vdots & \vdots & \ddots & \vdots & \vdots \\ 0 & 0 & 0 & 0 & \cdots & \mathbf{rr}_{1,1} & 0 \\ 0 & 0 & 0 & 0 & \cdots & 0 & \mathbf{rr}_{0,0} \end{bmatrix}, \tag{37}$$

where

$$\mathbf{rr}_{i,i} = 1 - \mathbf{rf}_{i,1},\ \forall\, 0 \le i \le \mathrm{m}. \tag{38}$$

4.1.6 Steady-State Probabilities

Let $\mathbf{P} = [p_1\ p_2\ ...\ p_{\mathbb{N}}]$ be the matrix of steady-state probabilities, where p_i is the probability of the i-th state in the equilibrium. Generally, following Markov chain theory, we have

$$\begin{cases} \mathbf{P} = \mathbf{PQ}, \\ \sum_{i=1}^{\mathbb{N}} p_i = 1, \end{cases} \tag{39}$$

where $\mathbf{Q}$ is the transition matrix obtained in (27).

In order to find the elements of $\mathbf{P}$, we can transform (39) into a basic set of linear equations formed as: $\mathbf{Ax} = \mathbf{B}$ and then solve it by using standard Gaussian elimination. Here, $\mathbf{x} = [p_1\ p_2\ ...\ p_{\mathbb{N}}]^T$, $\mathbf{B} = [0\ 0\ ...\ 1]^T$ and $\mathbf{A} = [a_{ij}]_{\mathbb{N}\times\mathbb{N}}$ where a_{ij} is given as

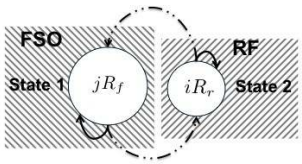

Fig. 6 The Markov chain for fixed rate systems.

$$\begin{cases} a_{ii} = q_{ii} - 1, \forall\ 1 \le i \le \mathbb{N}, \\ a_{ij} = q_{ij}, \forall\ 1 \le i \le \mathbb{N} - 1,\ 1 \le j \le \mathbb{N},\ i \ne j. \\ a_{\mathbb{N}j} = 1, \forall\ 1 \le j \le \mathbb{N}. \end{cases} \tag{40}$$

4.2 Markov Chain Model for Conventional Designs

In these designs, transmission rate of each link is fixed, and the link switching threshold is designed based on a target BER_0. We assume that a fixed M-QAM/N-PAM is adopted. There are two SNR thresholds obtained from (19) and (20): γ_{fj} and γ_{ri}, where $j = \log_2 N$, $i = \log_2 M$.

A Markov chain in Fig. 6 can be used to model the operation of the system. Notice that there are only two states. The system works on state 1 and state 2 when γ_f stays in $[\gamma_{fj}, \infty)$ and $[0, \gamma_{fj})$, respectively. The state transition and its elements are given as follows

$$\mathbf{Q} = \begin{bmatrix} q_{11} & q_{12} \\ q_{21} & q_{22} \end{bmatrix}, \tag{41}$$

$$q_{12} = \frac{N(\gamma_{fj})T_f^{(j)}}{1 - F_{\gamma_f}(\gamma_{fj})},\ q_{11} = 1 - q_{12}, \tag{42}$$

$$q_{21} = \frac{N(\gamma_{fj})T_r^{(i)}}{F_{\gamma_f}(\gamma_{fj})},\ q_{22} = 1 - q_{21}. \tag{43}$$

Finally, by applying (39) with $\mathbb{N} = 2$, all steady state probabilities (i.e., p_1 and p_2) can be obtained for the conventional designs.

5. Performance Metrics

We define several metrics to analytically study the performance of hybrid FSO/RF systems for AMR[1] (i.e., physical layer-based design), AMR[2] (i.e., AMR/ARQ cross-layer design), and the conventional designs. To illustrate the conventional designs, where transmission rate of each link is fixed, and the link switching threshold is designed based on a target BER_0, we assume that a fixed M-QAM/N-PAM is adopted.

For a fair comparison, the link layer ARQ for controlling frame re-transmissions is considered in all cases. It is important to note, however, that while in AMR[2] the switching thresholds depend on the persistence of ARQ; in other cases they are fixed.

5.1 Adaptive Multi-Rate

We first focus on deriving common closed-form expressions for performance parameters, which can be applied for both

AMR[1] and AMR[2] by using their own switching thresholds.

5.1.1 State Properties

When the system stays in a k-th state, it is characterized by several parameters, including steady-state probability (p_k), state transmission rate (R_k), and state frame-error rate (FER_k). While p_k and R_k are already discussed in the previous sections, the state frame-error rate is defined as follows

$$\begin{aligned}\text{FER}_k^{FSO} &= \frac{1}{p_k}\int_{\gamma_{fj}}^{\gamma_{f(j+1)}} \text{FER}(2^j,\gamma_f) f_{\gamma_f}(\gamma_f) d\gamma_f \\ &= \frac{1}{p_k}\left(\vartheta_f(\gamma_{f(j+1)}) - \vartheta_f(\gamma_{fj})\right), \end{aligned} \tag{44}$$

$$\begin{aligned}\text{FER}_k^{RF} &= \frac{1}{p_k}\int_{\gamma_{ri}}^{\gamma_{r(i+1)}} \text{FER}(2^i,\gamma_r) f_{\gamma_r}(\gamma_r) d\gamma_r \\ &= \frac{1}{p_k}\left(\vartheta_r(\gamma_{r(i+1)}) - \vartheta_r(\gamma_{ri})\right), \end{aligned} \tag{45}$$

where $[\gamma_{fj}, \gamma_{f(j+1)})$ (or $[\gamma_{ri}, \gamma_{r(i+1)})$) is the corresponding range operation of the k-th state in the FSO (or RF) link. In addition, we define

$$\vartheta_f(\gamma_{fj}) = \int_0^{\gamma_{fj}} \text{FER}(2^j,\gamma_f) f_{\gamma_f}(\gamma_f) d\gamma_f, \tag{46}$$

$$\vartheta_r(\gamma_{ri}) = \int_0^{\gamma_{ri}} \text{FER}(2^i,\gamma_r) f_{\gamma_r}(\gamma_r) d\gamma_r, \tag{47}$$

and their closed-form expressions are given in (48) and (49). The derivation for these equations can be found in the Appendixes.

5.1.2 Frame-Error Rate

The average FER is defined as the ratio of the average number of erroneously received packets over the total average number of transmitted packets, as follows

$$\overline{\text{FER}} = \frac{\sum_{k=1}^{\mathbb{N}} R_k p_k \text{FER}_k}{\sum_{k=1}^{\mathbb{N}} R_k p_k}. \tag{50}$$

Since ARQ with the persistence level of Ł is implemented at the link layer, with the average FER in (50), the actual FER is given as

$$\mathbf{FER} = \overline{\text{FER}}^{\text{Ł}+1}. \tag{51}$$

5.1.3 Average Link Layer Goodput

Average goodput is defined as the average number of successfully bits transmitted per unit time. We also consider the effects of ARQ re-transmissions in the definition of goodput as follows

$$\mathbf{G} = \frac{(1-\mathbf{FER})\overline{R}}{1+\overline{\text{Ł}}}, \tag{52}$$

where $\overline{R}$ and $\overline{\text{Ł}}$ are the average transmission rate and the average number of re-transmissions per frame, respectively. These parameters are given by

$$\overline{R} = \sum_{k=1}^{\mathbb{N}} R_k p_k, \; \overline{\text{Ł}} = \sum_{v=0}^{\text{Ł}} v\overline{\text{FER}}^v(1-\overline{\text{FER}}). \tag{53}$$

5.1.4 Link Switching Probability

In FSO/RF systems, the link switching probability is defined as the probability that the system stays in RF link [8]. So, this can be calculated as

$$\mathbf{P}_{sw} = \sum_{k=\mathbb{n}+1}^{\mathbb{N}} p_k. \tag{54}$$

5.2 Conventional Designs

Similar to the adaptive multi-rate cases, the states are characterized by (p_k, R_k, FER_k), where $1 \le k \le 2$. In here, $R_1 = jR_f$, $R_2 = iR_r$, and p_k is already discussed in Section 4.2. In addition, the mode frame-error rates are defined as

$$\text{FER}_1 = \frac{1}{p_1}\int_{\gamma_{fj}}^{\infty} \text{FER}(2^j,\gamma_f) f_{\gamma_f}(\gamma_f) d\gamma_f = \frac{\vartheta_f^*(\gamma_{fj})}{p_1}, \tag{55}$$

$$\text{FER}_2 = \frac{1}{p_2}\int_{0}^{\infty} f_{\gamma_r}(\gamma_r)\text{FER}(2^i,\gamma_r) d\gamma_r = \frac{\vartheta_r^*}{p_2}, \tag{56}$$

where the derivation for $\vartheta_f^*(\gamma_{fj})$ and ϑ_r^* can be found in the Appendixes.

Finally, by applying (51), (52) and (54) with $\mathbb{N} = 2$, all performance parameters can be obtained for the conventional designs.

$$\vartheta_f(\gamma_{fj}) = \frac{(2^j-1)l}{j2^j}\sum_{t=1}^{T}\left\{\frac{a_t B(\alpha-\beta,1-\alpha+\beta)}{2g_t^{\frac{\beta+\alpha}{2}}\Gamma(\alpha)\Gamma(\beta)}\sum_{p=0}^{\infty}\left[\frac{a_p(\alpha,\beta)}{\overline{\gamma}_f^{\frac{p+\beta}{2}}}\Gamma_l(\frac{p+\beta}{2}, g_t\gamma_{fj}) - \frac{a_p(\beta,\alpha)}{\overline{\gamma}_f^{\frac{p+\alpha}{2}}}\Gamma_l(\frac{p+\alpha}{2}, g_t\gamma_{fj})\right]\right\}, \tag{48}$$

$$\vartheta_r(\gamma_{ri}) = \frac{0.2l(K+1)}{\overline{\gamma}_r e^K}\sum_{q=0}^{\infty}\frac{(-1)^q}{q!\Gamma(q+1)}\frac{\left[\frac{K(K+1)}{\overline{\gamma}_r}\right]^q}{\left[\frac{3}{2(2^i-1)}+\frac{K+1}{\overline{\gamma}_r}\right]^{q+1}}\Gamma_l\left(q+1, \left[\frac{3}{2(2^i-1)}+\frac{K+1}{\overline{\gamma}_r}\right]\gamma_{ri}\right). \tag{49}$$

6. Numerical Results and Discussions

In this section, using the previously derived formulations, we present selected numerical results illustrating the performance of hybrid FSO/RF link for analyzed cases. For the AMRs, $\mathfrak{m} = \mathfrak{n} = 5$ is assumed. For the conventional designs, a fixed M-QAM/N-PAM with $M = N = 2, 4, 8, 16, 32$ is adopted. Moreover, for AMR[1] and conventional designs, where thresholds are designed independently of the persistence of ARQ, a fixed value of $Ł = 2$ is assumed, while for AMR[2], $Ł$ varying from 1 to 4 is assumed. In addition, we assume the atmospheric coherence time $t_0 = 1$ ms, the frame size $l = 1080$ bits, the symbol rates $R_f = 200$ Msps and $R_r = 30$ Msps[†], the target bit error rate $\mathrm{BER}_0 = 10^{-5}$. For fading channels, the Ricean factor $K = 6$ dB, which corresponds to the Ricean fading channel in RF link, and the Rytov variance $\sigma_R^2 = 0.9$, which corresponds to the moderate turbulence-induced fading in FSO link, are assumed. The following numerical results obtained by (51), (52), and (54) are plotted as a function of the average electrical SNR per symbol of FSO link, $\overline{\gamma}_f$, and the average electrical SNR per symbol of RF link, $\overline{\gamma}_r$.

Figure 7 depicts the average link layer goodput performance for the AMR[1] system and a fixed rate system with 32-PAM/32-QAM. In both systems, at high SNR of FSO link the system could achieve high goodput by operating on the FSO link, whereas at the low SNR the system tends to operate in the RF link and thus achieving a low goodput. However, the changing between these levels is different in two cases. Particularly, in Fig. 7(a), due to adaptive multi-rate scheme, we can remain a smooth change between low and high goodput levels. In Fig. 7(b), due to the fact that there are only two transmission rate levels, a sudden change may happen when SNR varies. Moreover, in this figure, there exists a large zero-goodput region where the goodput nearly drops to zero. For example, the goodput distribution surface corresponds to $\left\{\overline{\gamma}_f, \overline{\gamma}_r \mid \overline{\gamma}_f < 30\ \mathrm{dB}, \overline{\gamma}_r < 25\ \mathrm{dB}\right\}$.

Next, for further comparisons, in Fig. 8, we consider the average link layer goodput as a function of a common SNR defined as $\overline{\gamma} = \overline{\gamma}_f = \overline{\gamma}_r$. More importantly, we also compare the performance of AMR[2] with different values of the persistent level and fixed-rate systems with different values of modulation order. In fixed-rate cases, there are remarkable points: (i) a system with high-order modulation may achieves high maximum goodput (e.g., $\mathbf{G}_{max} = 1000$ Mbps when $M = N = 32$), yet it has a large zero-goodput region, and (ii) a system with low-order modulation may achieves low maximum goodput (e.g., $\mathbf{G}_{max} = 200$ Mbps when $M = N = 2$), yet it has a small zero-goodput region. Therefore, it is hard to determine the fixed-rate system that can simultaneously offer high maximum goodput and small zero-goodput region.

On the other hand, compared to the fixed-rate cases, AMRs have significantly better performance thanks to the

[†]Due to this setting, the maximum transmission rate of FSO link and RF link is 1000 Mbps and 150 Mbps, respectively. These values are selected as an illustrative example; it, however, is possible to illustrate a higher range by setting higher values of R_f and R_r.

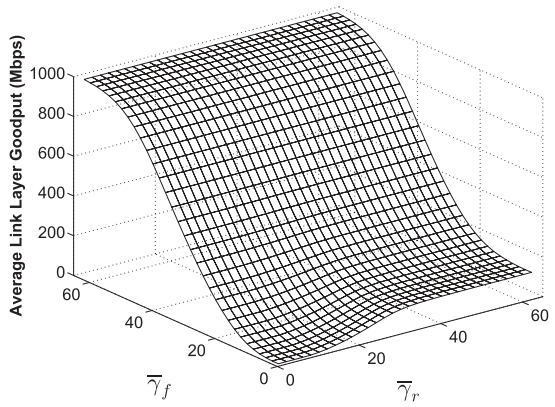

(a) Adaptive multi-rate system with physical layer-based design.

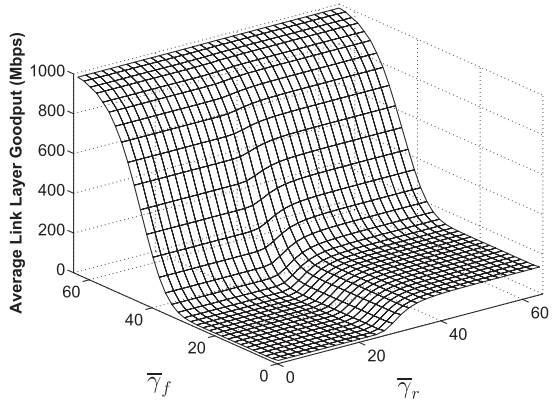

(b) Fixed rate system with 32-PAM/32-QAM.

Fig. 7 Average link layer goodput versus the average electrical SNR per symbol of FSO link $\overline{\gamma}_f$ and RF link $\overline{\gamma}_r$.

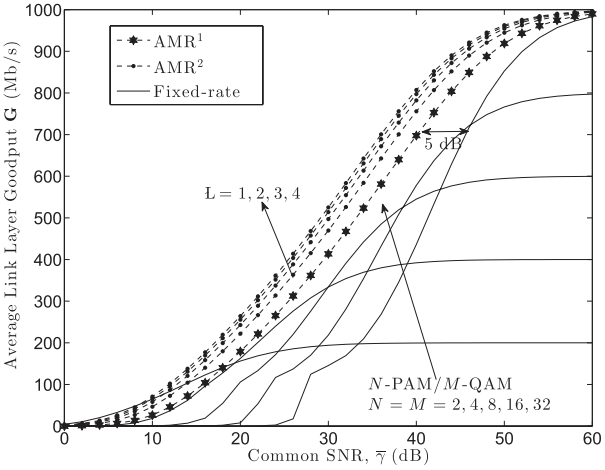

Fig. 8 Average link layer goodput versus the common SNR $\overline{\gamma}$.

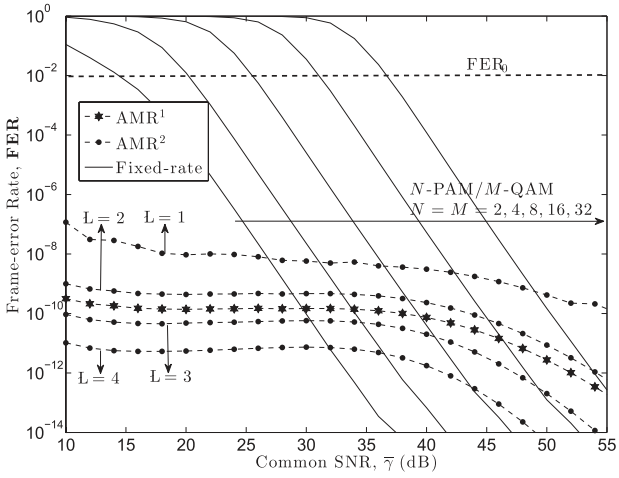

Fig. 9 Frame-error rate versus the common SNR $\overline{\gamma}$.

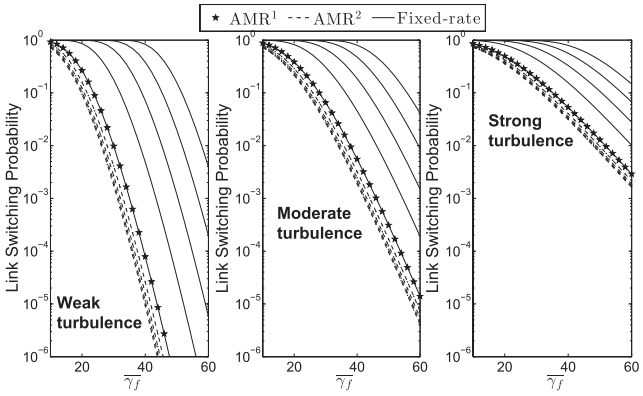

Fig. 10 Link switching probability versus the average electrical SNR per symbol of FSO link $\overline{\gamma}_f$.

adaptive multi-rate strategy. For example, to achieve the goodput of 700 Mbps, compared to the system with fixed 32-PAM/32-QAM, the system with AMR^1 offers more than 5-dB gain. Furthermore, the comparison of AMRs shows that AMR^2 performs more efficiently than AMR^1. It is also seen that the increase of persistence level further improves the goodput. The improvement is due to the cross-layer design.

Figure 9 emphasize the advantage of AMRs in terms of improving the reliability of system. The actual FER, corresponding to the different cases depicted in Fig. 8, are shown. Obviously, both proposed deigns have the stable FER, which is always lower than the target FER$_0$ (i.e., $l \times \text{BER}_0 = 10^{-5} \times 1080 \approx 10^{-2}$). This phenomenon does not happen in fixed-rate cases, especially with high-order modulations.

Next, we analyze the link switching probability in Fig. 10. As the link switching operates only based on the instantaneous received SNR of FSO link, we consider the link switching probability versus $\overline{\gamma}_f$. In addition, for fixed-rate systems, only modulation order of PAM is considered; in all cases, the modulation order ($N = 1, 2, 3, 4, 5$) increases from left to right. As is evident, for fixed-rate systems, operating in a low modulation order may help decrease the link switching probability. For example, with lowest modulation orders, $M = N = 2$, the link switching probability of fixed-rate system is compatible with AMR^1. However, as proved previously, the low modulation order causes low maximum goodput.

More importantly, we also investigate the effects of atmospheric turbulence on the link switching probability performance. We assume $\sigma_R^2 = 0.59$, $\sigma_R^2 = 0.9$, and $\sigma_R^2 = 1.2$ for the weak, moderate and strong turbulence conditions, respectively. Obviously, the atmospheric turbulence greatly affects on the system performance. For example, to keep the link switching probability under 10^{-2}, the required SNRs (with AMR^2 and Ł = 3) are higher than 27 dB, 35 dB and 42 dB corresponding to the weak, moderate and strong turbulence conditions, respectively. For a given SNR and turbulence conditions, comparing the designs, AMR^2 always achieves the best performance.

Finally, as in the cross-layer design, the key parameter reflecting the operation of ARQ is the persistence level, we summarize the effect of this parameter on the performance of AMR^2 from Figs. 8–10. Obviously, higher value of persistence level will result in better performance. However, the improvement increases slowly in high value of Ł. Note that, in practical implementation, a small value of Ł can help the transmitter manage frame transmissions more simply, and it may also incur lower delay and energy consumption [19]. We therefore highly recommend AMR^2 with Ł = 3 for practical systems.

7. Conclusions

We have proposed the concept of AMR for hybrid FSO/RF switchover systems to enhance overall system performance. We discussed two designs for AMR switching thresholds. A Markov chain model was presented to theoretically analyze the system performance. Closed-form expressions of system performance parameters of proposed designs and conventional designs were derived over fading channels. The results showed that compared to the fixed-rate cases, AMRs have significantly better performance, and among AMRs the cross-layer design in general performs more efficiently than the physical layer-based one. In addition, it was found that the recommended value of persistence level is 3 for the cross-layer design.

Acknowledgement

This research is supported in part by the University of Aizu Competitive Research Funding in the AY2014.

References

[1] X. Zhu and J.M. Kahn, "Free-space optical communication through atmospheric turbulence channels," IEEE Trans. Commun., vol.50, no.8, pp.1293–1300, Aug. 2002.
[2] F. Nadeem, V. Kvicera, M. Awan, E. Leitgeb, S. Muhammad, and G.

Kandus, "Weather effects on hybrid FSO/RF communication link," IEEE J. Sel. Areas. Commun., vol.27, no.9, pp.1687–1697, Dec. 2009.
[3] A. Eslami, S. Vangala, and H. Pishro-Nik, "Hybrid channel codes for efficient FSO/RF communication systems," IEEE Trans. Commun., vol.58, no.10, pp.2926–2938, Oct. 2010.
[4] D.M. Forin, G. Incerti, G.M. Tosi Beleffi, A.L.J. Teixeira, L.N. Costa, P.S. De Brito André, B. Geiger, E. Leitgeb and F. Nadeem, "Free space optical technologies," INTECH Open Access, 2010.
[5] B. He and R. Schober, "Bit-interleaved coded modulation for hybrid RF/FSO systems," IEEE Trans. Commun., vol.57, no.12, pp.3753–3763, Dec. 2009.
[6] N.D. Chatzidiamantis, G.K. Karagiannidis, E.E. Kriezis, and M. Matthaiou, "Diversity combining in hybrid RF/FSO systems with PSK modulation," Proc. 2011 IEEE International Conference on Communications (ICC), pp.1–6, June 2011.
[7] Y. Tang, M. Brandt-Pearce, and S.G. Wilson, "Link adaptation for throughput optimization of parallel channels with application to hybrid FSO/RF systems," IEEE Trans. Commun., vol.60, no.9, pp.2723–2732, Sept. 2012.
[8] H. Moradi, M. Falahpour, H.H. Refai, P.G. LoPresti, and M. Atiquzzaman, "Reconfiguration modeling of reconfigurable hybrid FSO/RF links," Proc. 2010 IEEE International Conference on Communications, pp.1–5, May 2010.
[9] F. Nadeem, M. Loeschnig, B. Geiger, G. Kandus, E. Leitgeb, and S.S. Muhammad, "Comparison of link selection algorithms for free space optics/radio frequency hybrid network," IET Communications, vol.5, no.18, pp.2751–2759, Dec. 2011.
[10] I.E. Lee, Z. Ghassemlooy, W.P. Ng, V. Gourdel, M.A. Khalighi, S. Zvanovec, and M. Uysal, "Practical implementation and performance study of a hard-switched hybrid FSO/RF link under controlled fog environment," Proc. 2014 9th International Symposium on Communication Systems, Networks & Digital Sign (CSNDSP), pp.368–373, July 2014.
[11] M. Usman, H.-C. Yang, and M.-S. Alouini, "Practical switching-based hybrid FSO/RF transmission and its performance analysis," IEEE Photonics J., vol.6, no.5, pp.1–13, Oct. 2014.
[12] F.F. Digham and M.-S. Alouini, "Variable-rate variable-power hybrid M-FSK M-QAM for fading channels," Proc. 2003 IEEE 58th Vehicular Technology Conference, VTC 2003-Fall (IEEE Cat. No.03CH37484), Vol.3, pp.1512–1516, Oct. 2003.
[13] M. Taki, M. Rezaee, and M. Guillaud, "Adaptive modulation and coding for interference alignment with imperfect CSIT," IEEE Trans. Wireless Commun., vol.13, no.9, pp.5264–5273, Sept. 2014.
[14] I.B. Djordjevic, "Adaptive modulation and coding for free-space optical channels," J. Opt. Commun. Netw., vol.2, no.5, pp.221–229, May 2010.
[15] N.D. Chatzidiamantis, A.S. Lioumpas, G.K. Karagiannidis, and S. Arnon, "Adaptive subcarrier PSK intensity modulation in free space optical systems," IEEE Trans. Commun., vol.59, no.5, pp.1368–1377, May 2011.
[16] M.Z. Hassan, M.J. Hossain, and J. Cheng, "Performance of non-adaptive and adaptive subcarrier intensity modulations in gamma-gamma turbulence," IEEE Trans. Commun., vol.61, no.7, pp.2946–2957, July 2013.
[17] S.M. Aghajanzadeh and M. Uysal, "Information theoretic analysis of hybrid-ARQ protocols in coherent free-space optical systems," IEEE Trans. Commun., vol.60, no.5, pp.1432–1442, May 2012.
[18] E. Zedini, A. Chelli, and M.-S. Alouini, "On the performance analysis of hybrid ARQ with incremental redundancy and with code combining over free-space optical channels with pointing errors," IEEE Photonics J., vol.6, no.4, pp.1–18, Aug. 2014.
[19] V.V. Mai and A.T. Pham, "Performance analysis of cooperative-ARQ schemes in free-space optical communications," IEICE Trans. Commun., vol.E97-B, no.8, pp.1614–1622, 2014.
[20] M.K. Simon and M.S. Alouini, Digital Communication over Fading Channels, 2nd ed., Wiley-IEEE Press, Nov. 2004.
[21] B.T. Teipen, M.H. Eiselt, K. Grobe, and J.-P. Elbers, "Adaptive data rates for flexible transceivers in optical networks," J. Networks, vol.7, no.5, pp.776–782, 2012.
[22] A. Puryear, R. Jin, E. Lee, and V.W.S. Chan, "Experimental analysis of the time dynamics of coherent communication through turbulence: Markovianity and channel prediction," Proc. 2011 International Conference on Space Optical Systems and Applications (ICSOS), pp.28–37, May 2011.
[23] H.S. Wang and N. Moayeri, "Finite-state Markov channel-a useful model for radio communication channels," IEEE Trans. Veh. Technol., vol.44, no.1, pp.163–171, Feb. 1995.
[24] K.P. Peppas and C.K. Datsikas, "Average symbol error probability of general-order rectangular quadrature amplitude modulation of optical wireless communication systems over atmospheric turbulence channels," J. Opt. Commun. Netw., vol.2, no.2, pp.102–110, Feb. 2010.
[25] M. Chiani, D. Dardari, and M.K. Simon, "New exponential bounds and approximations for the computation of error probability in fading channels," IEEE Trans. Wireless Commun., vol.2, no.4, pp.840–845, July 2003.
[26] E. Bayaki, R. Schober, and R. Mallik, "Performance analysis of MIMO free-space optical systems in gamma-gamma fading," IEEE Trans. Commun., vol.57, no.11, pp.3415–3424, Nov. 2009.

Appendix A: Derivations of $\vartheta_f(\gamma_{fj})$

We first use a approximation for erfc(.):

$$\mathrm{erfc}(x) = \sum_{t=1}^{T} a_t \exp(-b_t x^2), \tag{A·1}$$

where $T \in \mathbb{Z}^+$, $a_t = \frac{2(\theta_t - \theta_{t+1})}{\pi}$, $b_t = \frac{1}{\sin^2\theta_t}$, $\theta_t = \frac{t\pi}{2T}$ [25]. So, $\mathrm{FER}(2^j, \gamma_f)$ can be rewritten as

$$\mathrm{FER}(2^j, \gamma_f) = \frac{(2^j - 1)l}{j2^j} \sum_{t=1}^{T} a_t \exp(-g_t \gamma_f), \tag{A·2}$$

where $g_t = \frac{3b_t}{2(2^j-1)(2^{j+1}-1)}$. Substituting (A·2) to (46), we have

$$\vartheta_f(\gamma_{fj}) = \frac{(2^j - 1)l}{j2^j} \sum_{t=1}^{T} \int_0^{\gamma_{fj}} a_t \exp(-g_t \gamma_f) f_{\gamma_f}(\gamma_f) d\gamma_f. \tag{A·3}$$

Now, using a series expansion of the modified Bessel function of second kind [26],

$$K_v(y) = \frac{\pi}{2\sin(\pi v)} \sum_{p=0}^{\infty} \left[\frac{(y/2)^{2p-v}}{\Gamma(p - v + 1)p!} - \frac{(y/2)^{2p+v}}{\Gamma(p + v + 1)p!}\right], v \notin \mathbb{Z}, |y| < \infty, \tag{A·4}$$

we rewrite $f_{\gamma_f}(\gamma_f)$ as

$$f_{\gamma_f}(\gamma_f) = \frac{B(\alpha - \beta, 1 - \alpha + \beta)}{2\Gamma(\alpha)\Gamma(\beta)} \sum_{p=0}^{\infty} \left[\frac{a_p(\alpha, \beta)}{\overline{\gamma}_f^{\frac{p+\beta}{2}}} \gamma_f^{\frac{p+\beta-2}{2}} - \frac{a_p(\beta, \alpha)}{\overline{\gamma}_f^{\frac{p+\alpha}{2}}} \gamma_f^{\frac{p+\alpha-2}{2}}\right], \tag{A·5}$$

where $a_p(x, y)$ is given by

$$a_p(x,y) = \frac{(xy)^{p+y}}{\Gamma(p-x+y+1)p!}. \quad (A\cdot 6)$$

Let's define $\wp_f = \int_0^{\gamma_{fj}} a_t \exp(-g_t\gamma_f) f_{\gamma_f}(\gamma_f) d\gamma_f$. By using (A· 5), making the change of variable $k = g_t\gamma_f$, and then applying the lower incomplete Gamma function, $\Gamma_l(m,x) = \int_0^x k^{m-1}\exp(-k)dk$, we can obtain the closed-form expression of $\wp_f$, that is

$$\wp_f = \frac{a_t B(\alpha-\beta, 1-\alpha+\beta)}{2g_t^{\frac{\beta+\alpha}{2}}\Gamma(\alpha)\Gamma(\beta)} \sum_{p=0}^{\infty} [\frac{a_p(\alpha,\beta)}{\overline{\gamma}_f^{\frac{p+\beta}{2}}} \Gamma_l(\frac{p+\beta}{2}, g_t\gamma_{fj}) - \frac{a_p(\beta,\alpha)}{\overline{\gamma}_f^{\frac{p+\alpha}{2}}} \Gamma_l(\frac{p+\alpha}{2}, g_t\gamma_{fj})]. \quad (A\cdot 7)$$

Finally, submitting (A· 7) to (A· 3), we achieve (48). In this equation, according to [25] and [26], we run p from 0 to 40, and t from 1 to 3 to have a good accuracy.

Appendix B: Derivations of $\vartheta_r(\gamma_{ri})$

Using (8) and a series expansion of the modified Bessel function of first kind for the zero order, we obtain

$$f_{\gamma_r}(\gamma_r) = \frac{K+1}{\overline{\gamma}_r}\exp\left(-K-(K+1)\frac{\gamma_r}{\overline{\gamma}_r}\right) \times \sum_{q=0}^{\infty} \frac{(-1)^q}{q!\Gamma(q+1)}\left[K(K+1)\frac{\gamma_r}{\overline{\gamma}_r}\right]^q. \quad (A\cdot 8)$$

Substituting (A· 8) and (23) to (47), we have

$$\vartheta_r(\gamma_{ri}) = \frac{0.2l(K+1)}{\overline{\gamma}_r e^K} \times \sum_{q=0}^{\infty} \frac{(-1)^q}{q!\Gamma(q+1)} \int_0^{\gamma_{ri}} (b\gamma_r)^q \exp(-a\gamma_r)\, d\gamma_r, \quad (A\cdot 9)$$

where

$$a = \frac{3}{2(2^i-1)} + \frac{K+1}{\overline{\gamma}_r}, \quad b = \frac{K(K+1)}{\overline{\gamma}_r}. \quad (A\cdot 10)$$

Let's define $\wp_r = \int_0^{\gamma_{ri}} (b\gamma_r)^q \exp(-a\gamma_r)\, d\gamma_r$. By making the change of variable $k = a\gamma_r$, and then applying the lower incomplete Gamma function, we can obtain

$$\wp_r = \frac{b^q}{a^{q+1}}\Gamma_l(q+1, a\gamma_{ri}). \quad (A\cdot 11)$$

Finally, substituting (A· 10) and (A· 11) to (A· 9), we achieve (49).

Appendix C: Derivations of $\vartheta_f^*(\gamma_{fj})$

$\vartheta_f^*(\gamma_{fj})$ can be derived as same way of $\vartheta_f(\gamma_{fj})$. To change the interval of integration from $[0,\gamma_{fj}]$ to $[\gamma_{fj},\infty)$, we use the upper incomplete Gamma function, $\Gamma_u(m,x) = \int_x^{\infty} k^{m-1}\exp(-k)dk$. So, By replacing $\Gamma_l(.,.)$ by $\Gamma_u(.,.)$ in (48), we get the closed-form expression of $\vartheta_f^*(\gamma_{fj})$.

Appendix D: Derivations of ϑ_r^*

ϑ_r^* can be derived as same way of $\vartheta_r(\gamma_{ri})$. To change the interval of integration from $[0,\gamma_{ri}]$ to $[0,\infty)$, we use the ordinary gamma function, $\Gamma(m) = \int_0^{\infty} k^{m-1}\exp(-k)dk$. So, By replacing $\Gamma_l\left(q+1, \left[\frac{3}{2(2^i-1)} + \frac{K+1}{\overline{\gamma}_r}\right]\gamma_{ri}\right)$ by $\Gamma(q+1)$ in (49), we get the closed-form expression of ϑ_r^*.

Vuong V. Mai received the B.E. degree in Electronic Telecommunication Engineering from Posts and Telecommunications Institute of Technology, Vietnam in 2012, and the M.E. degree in Computer Network System from The University of Aizu (UoA), Japan in 2014. He is currently working toward a Ph.D. degree in Computer Science and Engineering at UoA. Mai's study in Japan is funded by a Japanese government scholarship (MonbuKagaku-sho). His current research focuses on cross-layer design and performance analysis for Optical Wireless Communications. Mai is student member of IEEE and IEICE.

Anh T. Pham received the B.E. and M.E. degrees, both in Electronics Engineering from the Hanoi University of Technology, Vietnam in 1997 and 2000, respectively, and the Ph.D. degree in Information and Mathematical Sciences from Saitama University, Japan in 2005. From 1998 to 2002, he was with the NTT Corp. in Vietnam. Since April 2005, he has been on the faculty at the University of Aizu, where he is currently a Professor of Computer Communications with the Division of Computer Engineering. Dr. Pham also holds an adjunct professor position at Vietnam National University/University of Engineering and Technology. Dr. Pham's research interests are in the broad areas of communication theory and networking with a particular emphasis on modeling, design and performance evaluation of wired/wireless communication systems and networks. He received Japanese government scholarship (MonbuKagaku-sho) for Ph.D. study. He also received Vietnamese government scholarship for undergraduate study. Dr. Pham is senior member of IEEE. He is also member of IEICE and OSA.